ORIGINAL
RESEARCH

T. Okada
Y. Miki
K. Kikuta
N. Mikuni
S. Urayama
Y. Fushimi
A. Yamamoto
N. Mori
H. Fukuyama
N. Hashimoto
K. Togashi

Diffusion Tensor Fiber Tractography for Arteriovenous Malformations: Quantitative Analyses to Evaluate the Corticospinal Tract and Optic Radiation

BACKGROUND AND PURPOSE: We hypothesized that diffusion tensor fiber tractography would be affected by intracranial arteriovenous malformation (AVM). The purpose of the present study was to evaluate the influence of intracranial AVM on corticospinal tract and optic radiation tractography.

MATERIALS AND METHODS: The subject group comprised 34 patients with untreated intracranial AVM. Hemorrhage was present in 13 patients and absent in 21 patients. Perinidal fractional anisotropy (FA) and number of voxels along the reconstructed corticospinal and optic radiation tracts were measured, and left-to-right asymmetry indices (AIs) for those values were quantified. Patients were assigned to 1 of 3 groups: tracts distant from nidus, tracts close to nidus without neurologic symptoms, and tracts close to nidus associated with neurologic symptoms. One-way analysis of variance was used to compare differences in AI between groups. Hemorrhagic and nonhemorrhagic groups were assessed separately.

RESULTS: In patients without hemorrhage, AI of optic radiation volume ($P < .0001$), AI of perinidal FA along corticospinal tract ($P = .006$), and optic radiation ($P = .01$) differed significantly between groups. In patients associated with hemorrhage, AI of corticospinal tract volume ($P = .01$), AI of perinidal FA along corticospinal tract ($P = .04$), and optic radiation ($P = .004$) differed significantly between groups.

CONCLUSIONS: Corticospinal tract and optic radiation tractography were visualized in patients with AVM. In patients with both hemorrhagic and nonhemorrhagic AVM, the 2 fiber tracts close to the nidus were less visualized in the affected hemisphere than those distant from the nidus. Tracts were less visualized in patients with neurologic symptoms than in asymptomatic patients.

Diffusion tensor (DT) imaging and fiber tractography can visualize 3D macroscopic fiber tract architectures.[1-3] These techniques offer information about eloquent white matter tracts in patients with brain tumors.[4,5] Among eloquent fiber tracts, locations of the corticospinal tract for motor pathways and the optic radiation for visual pathways are the most important based on clinical demands. DT fiber tractography in patients with intracranial arteriovenous malformation (AVM) has also been reported recently, and the usefulness and limitations of tractography in patients with AVM have been discussed.[6,7] However, changes to fiber tract visualization in patients with AVM have not been fully discussed. We hypothesized that the results of DT fiber tractography would be affected by AVM. Our purpose was to visualize corticospinal tract and optic radiation tractography in patients with intracranial AVM and to evaluate the influences of AVM on tractography. We applied quantitative analyses to delineate subtle changes derived from underlying pathology in DT tractography, which was reported recently to be useful in corticospinal tract tractography.[8]

Subjects and Methods

Patients

MR imaging was performed on 41 consecutive patients with intracranial AVM who presented to our institution between May 2004 and December 2005. Of these 41 patients, 6 patients were excluded because of metal artifact near the AVM nidus as a result of previous treatment, and another patient was excluded because of poor image quality attributable to acute large intracerebral hemorrhage and bulk motion. The subject group comprised the remaining 34 consecutive patients (18 men and 16 women; mean age, 34 years; range, 6–72 years) with intracranial AVM. All of the patients were diagnosed with AVM on the basis of cerebral angiography. Institutional review board approval was obtained for this study. Written informed consent was obtained from all of the adult patients and from the parents of the 4 pediatric patients. According to the Spetzler-Martin grading system, patients without hemorrhage were classified as follows: grade 1, 4 patients; grade 2, 9 patients; grade 3, 5 patients; grade 4, 3 patients; and grade 5, no patient. Similarly, patients associated with hemorrhage were as follows: grade 1, 1 patient; grade 2, 6 patients; grade 3, 4 patients; grade 4, 1 patient; and grade 5, 1 patient. Two experienced neurosurgeons performed neurologic examinations in all of the patients, including manual muscle testing and visual field examination, by using confrontation method. Patients suspected of visual field defect were confirmed with the use of Goldmann perimetry. Details of patient demographics are provided in Table 1.

Data Acquisition

MR imaging was performed using a whole-body 3T MR scanner (Trio; Siemens, Erlangen, Germany) equipped with a 40 mT/m gradient, integrated parallel acquisition technique, and a receiver-only

Table 1: Demographic data for 34 patients with untreated intracranial AVM

Patient No.	Sex	Age at MR Imaging (years)	Location of Nidus	Hemorrhage	Perifocal Hyperintensity	Neurologic Symptoms	Spetzler-Martin Grade
1	F	29	Right occipital	No	No	No	2
2	M	31	Right frontal	No	No	No	1
3	F	27	Left occipital	No	Yes	Right homonymous hemianopsia	3
4	M	64	Right occipital	No	No	No	2
5	M	49	Left frontal	No	Yes	No	2
6	M	72	Left parietal	No	No	No	1
7	M	25	Left occipital	No	No	No	2
8	M	45	Right frontal	No	Yes	No	3
9	M	28	Left frontal	No	No	No	3
10	M	49	Left putamen	No	No	No	2
11	M	25	Right temporal	No	Yes	No	2
12	M	28	Right occipital	No	No	Left lower quadranopsia	4
13	F	5	Left parietal	No	No	No	1
14	M	59	Right frontal	No	Yes	No	1
15	F	28	Right parietal	No	No	No	2
16	M	45	Left cingulum	No	No	No	2
17	F	33	Right cingulum	No	No	No	4
18	F	29	Left frontal	No	No	No	2
19	M	28	Right insula	No	No	No	4
20	F	17	Left cerebellum	No	Yes	Cerebellar ataxia	3
21	F	20	Left frontal	No	No	No	3
22	F	45	Right occipital	Yes	No	No	3
23	F	29	Left occipital	Yes	No	No	2
24	M	22	Right cerebellum	Yes	No	Cerebellar ataxia	4
25	F	15	Right occipital	Yes	No	No	3
26	F	56	Right cerebellum	Yes	Yes	Cerebellar ataxia, right trigeminal palsy	1
27	M	45	Right parietal	Yes	Yes	Recent memory disturbance	3
28	F	21	Right occipital	Yes	Yes	Left upper quadranopsia	2
29	F	27	Right parietal	Yes	Yes	Left hemianopsia	2
30	F	6	Right frontal	Yes	Yes	Left hemiparesis (MMT4/5)	2
31	M	38	Right parietal	Yes	No	Left hemiparesis (MMT 4/5)	2
32	M	50	Left frontal	Yes	Yes	Motor aphasia	5
33	F	23	Right frontal	Yes	Yes	Left hemiparesis (MMT 4/5)	2
34	M	48	Left parietal	Yes	Yes	Right hemiparesis (MMT 3/5), right spatial neglect	3

Note:—M indicates male; F, female; MMT, manual muscle testing. Patients 1–21 were without intracranial hemorrhage, and patients 22–34 displayed hemorrhage.

8-channel phased-array head coil. A single-shot spin-echo echo-planar sequence was applied for DT imaging with the following parameters: TR, 7000 ms; TE, 79 ms; motion-probing gradient in 40 non-colinear directions and 4 b = 0 scans; b value, 700 s/mm^2; matrix, 128 × 104; voxel size, 2 × 2 × 2 mm; no intersection gap; and single averaging. The generalized autocalibrating partial parallel acquisition (GRAPPA) algorithm was applied for parallel imaging, with a reduction factor of 2 and 24 additional autocalibrating phase-encoding lines in the center of k-space. Section planes were parallel to the anteroposterior commissure line. A total of 60 transverse sections covered the whole brain. Acquisition time was 5 minutes and 30 seconds. Whole-brain MR angiography was also obtained to identify the AVM nidus. The 3D time-of-flight technique was applied with the following parameters: TR, 22 ms; TE, 3.9 ms; flip angle, 20°; 5-slab acquisition with 44 sections per slab and 25% section oversampling; section thickness, 0.64 mm; matrix, 320 × 256; and voxel size, 0.63 × 0.63 × 0.64 mm. The GRAPPA algorithm was also applied for parallel imaging, with a reduction factor of 2 and an additional 36 autocalibrating phase-encoding lines in the center of k-space. Section planes and field center were the same as in DT imaging. Acquisition time was 4 minutes 8 seconds.

DT Imaging Data Processing and Fiber Tractography Reconstruction

DT imaging datasets were transferred in Digital Imaging and Communications in Medicine format to a Windows personal computer workstation. DTIStudio version 2.02 software (H. Jiang and S. Mori, Department of Radiology, Johns Hopkins University, Baltimore, Md) was used for tensor calculations.[9] The details of DT imaging data processing were described elsewhere.[10] Three eigenvalues and eigenvectors were obtained, and then fractional anisotropy (FA) maps and a directional color-coded map were synthesized.

Fiber tractography was performed on the basis of the fiber assignments derived by continuous tracking (FACT) method.[9] Tracking from all of the pixels inside the brain (ie, by using the brute force approach) was performed, initiated in both retrograde and orthograde directions according to the direction of the principal eigenvector in each voxel. Results that penetrated the ≥2 manually segmented regions of interests (ROIs) on the basis of known anatomic distributions of tracts were assigned to the specific tract (ie, with the multiple ROI approach), which is highly beneficial for reproducible reconstruction of prominent white matter tracts.[11] When multiple ROIs were used for tract reconstruction, 3 types of operation were applied: AND, OR, and NOT. Choice of operations depended on the characteristic trajectory of the tract. Propagation in each fiber tract was terminated if a voxel with an FA value of <0.2 was reached or if the turning angles of 2 consecutive vectors were >70° during tracking. A relatively large angle threshold was used so that the optic radiation coursing in acute angle at the Meyer loop could be reconstructed.[12,13]

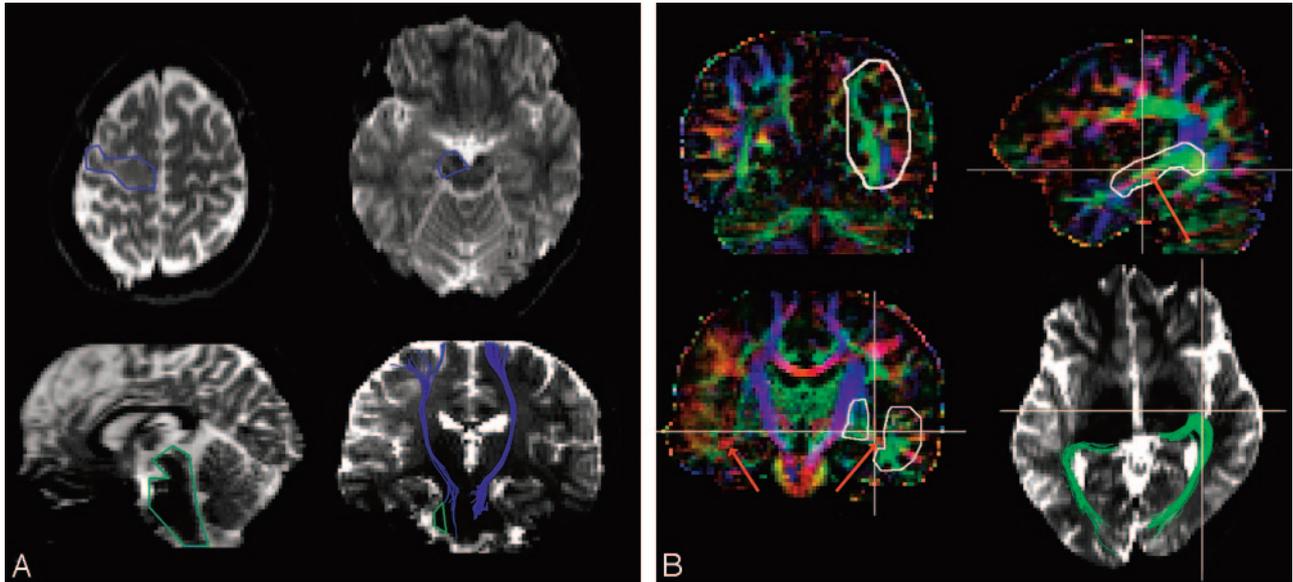To reconstruct corticospinal tract tractography, 2 ROIs were seg-

Fig 1. *A*, ROI segmentation for corticospinal tract tractography. Polygonal ROIs are placed on transverse b = 0 images (TR/TE, 7000 ms/79 ms). The first "OR" ROI (*blue*) is placed at either side of the cerebral peduncle on the plane where the characteristic Ω shape of the central sulcus is at the center of cerebral hemisphere (*top left*). The second "AND" ROI (*blue*) is placed at the ipsilateral precentral gyrus (*top right*). Left and right ROI segmentations were separately performed. "NOT" ROIs (*green*) are placed on midline structures connecting right and left corticospinal tracts on sagittal reconstructed image (*bottom left*) and fibers projecting into ipsilateral cerebellar peduncle on coronal reconstructed image (*bottom right*). Examples of bilateral corticospinal tract overlaid on coronal reconstructed image are shown (*bottom right*).

B, ROI segmentation for optic radiation tractography. The 4 kinds of ROIs (*white polygon*) are placed on coronal or sagittal color-coded maps. *Cross lines* indicate the orthogonal planes. The first "OR" ROI is placed at either side of the occipital lobe, including the calcarine cortex on the coronal plane through the anterior edge of the occipital-parietal sulcus (*top left*). The second "AND" ROI is placed at the ipsilateral temporal stem, including the Meyer loop on the sagittal plane (*top right*). Temporal stem is identified as *green*, and the Meyer loop is identified as a *small red area* inside the temporal stem (*red arrow*). The third and fourth "NOT" ROIs are placed on the same coronal plane through the dorsal end of the Sylvian fissure (*bottom left*). Bilateral Meyer loops are indicated as *red arrows*. Occipital-frontal connections medial to the Meyer loop and fibers projecting to the temporal horn passing through lateral to the Meyer loop are removed using the "NOT" operation. Examples of bilateral optic radiation overlaid on transverse b = 0 images (TR/TE, 7000 ms/79 ms) are shown (*bottom right*).

mented on transverse b = 0 images based on established anatomic landmarks. The first ROI was at either side of cerebral peduncle, whereas the second ROI was at the ipsilateral precentral gyrus.[4,8,10] The first ROI was segmented using an "OR" operation and the second ROI using an "AND" operation. Right and left tracts were separately segmented. Fibers connecting the right and left corticospinal tracts via transverse pontine connection and fibers projecting into cerebellar peduncles were then removed by using the "NOT" operation because of apparent lack of compliance with classic definitions of the corticospinal tract. Illustrative examples of ROIs and corticospinal tract are shown in Fig 1*A*.

Right and left optic radiations were also separately segmented. To reconstruct optic radiation tractography, the first "OR" ROI was placed on either side of the occipital lobe, including the calcaline cortex on coronal color-coded maps. The second "AND" ROI was at the ipsilateral temporal stem on sagittal color-coded mapping, including the Meyer loop. Most fibers in the temporal stem were green in the color-coded map, but the Meyer loop was red according to fiber direction and was distinguishable from other bundles. Various kinds of anteroposterior long association fibers or temporal projection fibers with diverting connectivity were included after these 2 ROI operations, such as the inferior occipitofrontal fasciculus and inferior longitudinal fasciculus. Based on the correlation between temporal fiber dissection and MR imaging,[14] 2 more "NOT" ROI operations were applied to the ipsilateral temporal stem on coronal color-coded maps. One was lateral and the other medial to the Meyer loop. As a result, optic radiation tractography along the sagittal stratum was delineated. Examples of ROIs and bilateral optic radiation are shown in Fig 1*B*. One author performed all of the ROI segmentations.

Data Analysis for Fiber Tractography

The distances between the margins of tractography and the margin of the AVM lesion (including nidus, hematoma, and draining vein) were measured on transverse b = 0 images. Sections for measurement were manually selected by 1 of the authors, where tractography appeared to be nearest to the margin. When the nidus was too small to be identified on b = 0 images (*n* = 3; Spetzler grade 1 AVM, *n* = 1 [patient 13]; Spetzler grade 2 AVM, *n* = 2 [patients 5 and 10]), images from MR angiography were referred. Subjects were assigned to 1 of the following groups according to measured distances and the presence of neurologic symptoms: group A, tracts distant from nidus; group B, tracts close to nidus without neurologic symptoms; and group C, tracts close to nidus associated with neurologic symptoms. Distances ≥1 cm between tracts and nidus were assigned "tracts distant from nidus" and <1 cm were assigned "tracts close to nidus." Motor weakness in the contralateral side was defined as neurologic symptom related to corticospinal tract damage, and visual field defect presented as contralateral hemianopsia or quadranopsia was defined as related to optic radiation damage. A group of representative patients are shown in Fig 2*A* (corticospinal tract) and Fig 2*B* (optic radiation). In these figures, depiction of tractography, vasculature, and lesion in 3D were performed by using Amira 4.0 software (Mercury Computer Systems, Chelmsford, Mass).

Various changes in tractographic appearances were observed in affected hemispheres. Tractographic appearances were classified into 4 categories: no change, compression, penetration, and disruption. Visually intact tract displaced by the lesion was defined as compression, intact tract propagating through the dilated nidal vessels was defined as penetration, and tract terminated near the lesion was de-
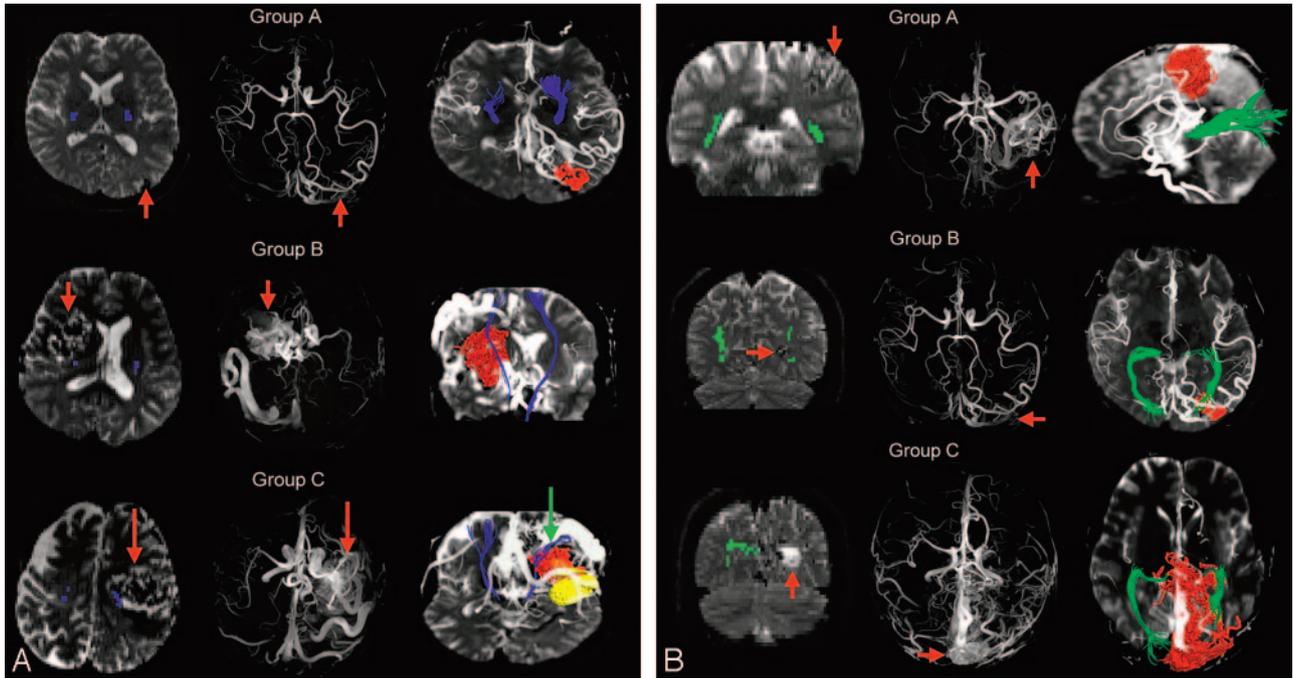
Fig 2. *A*, Corticospinal tract tractography. Patients were classified into 1 of 3 groups based on the distance between AVM nidus and tract and the presence of motor weakness. Three groups (*A–C*) are assigned from *top row* to *bottom row. Left column* displays transverse b = 0 images (TR/TE, 7000 ms/79 ms). *Blue areas* represent the voxel where fiber tracts penetrate the image. *Middle column* displays transverse maximum intensity projection (MIP) images of MR angiography. *Red arrows* indicate AVM nidus. *Right column* displays 3D reconstruction of fibers and MR angiography superimposed on b = 0 images. 3D reconstructions of AVM nidus (*red*) and hemorrhage (*yellow*) segmented from MR angiography were displayed by using shaded surface rendering. Patients in groups A and B are subjects without hemorrhage, and the group C patient is a subject with hemorrhage in this figure. In this group C patient, left corticospinal tract veers laterally, and projection fibers from the medial precentral gyrus are not visualized (*green arrow*).

B, Optic radiation tractography. Patients were classified into 1 of 3 groups based on the distance between AVM nidus and tract and the presence of visual field defect. Optic radiation tractography is represented in *green*, and imaging methods are the same as explained in *A*. The group B patient is the same as the group A patient presented in *A*. In this group C patient, left optic radiation was disrupted around the occipital pole.

fined as disruption. Numbers of patients in groups B and C for each tractographic appearances were counted.

To assess tractography quantitatively, 2 parameters were selected: FA of perinidal region and number of voxels along the tractography. Corticospinal tract damage was reported to correlate with FA along the tractography in patients with amyotrophic lateral sclerosis[8] or chronic ischemic stroke.[15] The number of voxels along the tractography represented the entire volume of tractography. These parameters were recorded by using a specific function of DTIStudio. Two ROIs were placed on the FA map, one in the tract located nearest to the AVM nidus, and the other in the contralateral tract of the same section. ROI for the corticospinal tract was segmented on an axial FA map and ROI for optic radiation on a coronal FA map. Each ROI has 9 oval-shaped 36-mm^2 pixels.

Although diffusion characteristics in the normal brain are somewhat asymmetrical, corticospinal tract tractography in healthy subjects reportedly displays little asymmetry.[16] To quantitatively evaluate mean FA and number of voxels along the tractography in affected hemispheres, asymmetry index (AI) of the 2 parameters between the affected and unaffected hemispheres was calculated by applying the following equation: the difference in parameters between unaffected and affected sides was divided by the mean of both sides {AI = (unaffected − affected)/[(unaffected + affected)/2]}, as described previously.[10] Index range was from −2 to 2.

For statistical analysis, 1-way analysis of variance was performed to compare differences in AIs of the mean FA and number of voxels along the tractography between each distance score. Hemorrhagic and nonhemorrhagic patients were assessed separately. Statistical

analyses were performed by using JMP5.1 software (SAS Institute, Cary, NC). Values of $P < .05$ were considered statistically significant.

Results

Corticospinal tract tractography was visualized in all of the patients. Regarding the distance between lesion and tractography in the affected hemisphere and motor weakness, results for patients without hemorrhage were as follows: group A, n = 14; group B, n = 7; and group C; n = 0. No patient with AVM close to corticospinal tract presented motor weakness. Among the 7 patients assigned to group B, corticospinal tract was compressed medially in 1 patient (patient 17), and the other patients displayed no remarkable shift or disruption. Similarly, results for patients associated with hemorrhage were as follows: group A, n = 7; group B, n = 2; and group C, n = 4. Corticospinal tract of 1 patient assigned to group B was compressed anteriorly (patient 29), and the other patient displayed no remarkable shift or disruption. Among the 4 patients assigned to group C, corticospinal tract in the affected hemisphere was veering laterally at the level of the centrum semiovale, and projection fibers from the medial precentral gyrus were disrupted in patient 34 (Fig 2*A, green arrow*). The corticospinal tract was compressed posteriorly in patient 33 and was not shifted or disrupted in the remaining 2 patients.

Optic radiation tractography was also visualized in all of the patients. Results for patients without hemorrhage were as follows: group A, n = 14; group B, n = 5; and group C; n = 2. Among the 5 patients assigned to group B, 2 tracts were com-

Table 2: Tractographic appearances and neurologic symptoms for corticospinal tract and optic radiation close to nidus

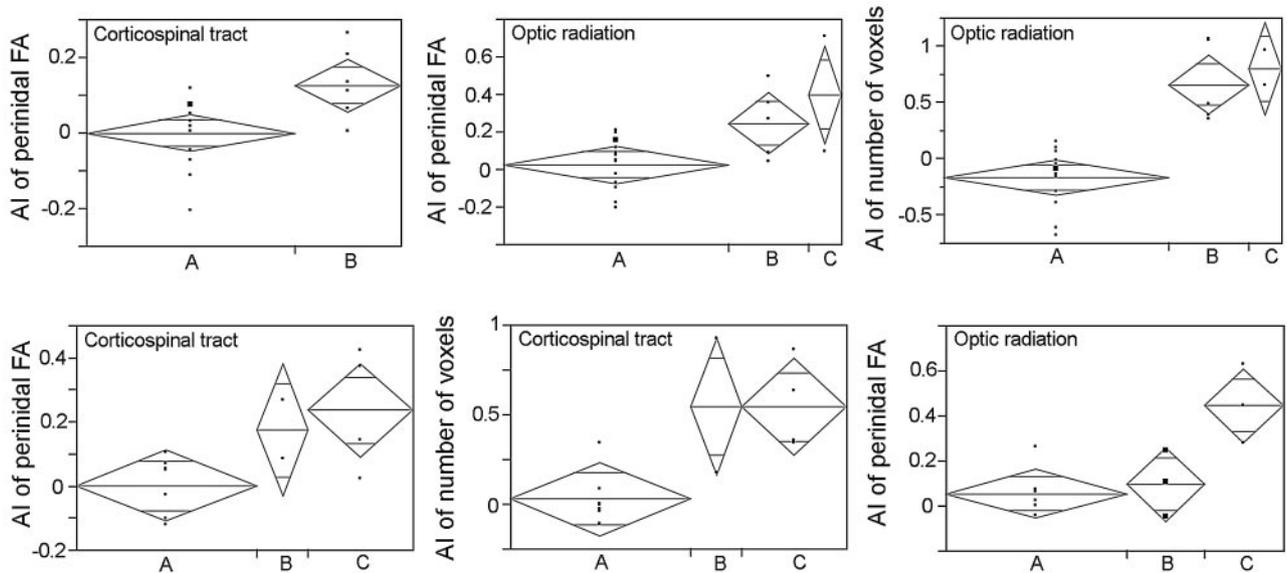| Variable	Group B		Group C	
	Nonhemorrhagic	Hemorrhagic	Nonhemorrhagic	Hemorrhagic
Corticospinal tract				
No change	6	0	0	2
Compression	1	2	0	1
Disruption	0	0	0	1
Optic radiation				
No change	1	1	1	1
Compression	2	1	0	2
Penetration	0	1	0	0
Disruption	2	0	1	0

Fig 3. Results of statistical analysis with significant differences are demonstrated. *Top row* displays patients without intracranial hemorrhage, and *bottom row* displays patients with intracranial hemorrhage. *Gray rhomboids* indicate mean and its 95% confident intervals. *Horizontal axes* represent groups A–C, and *vertical axes* represent AIs. In patients without intracranial hemorrhage, AI of perinidal FA along corticospinal tract (*left*, $P = .006$) and optic radiation (*middle*, $P = .01$) and AI of optic radiation volume (*right*, $P < .0001$) differed significantly between groups. In patients with hemorrhage, AIs of perinidal FA ($P = .04$), tract volume ($P = .01$) of corticospinal tract, and AI of perinidal FA along optic radiation ($P = .004$) differed significantly between groups.

pressed by the nidus (patients 1 and 15), 2 were disrupted by the nidus (patients 4 and 7), and the remaining patient displayed no remarkable shift or disruption. Optic radiation of one patient assigned to group C was disrupted (patient 3), and the other patient displayed no remarkable shift or disruption. Similarly, results for patients associated with hemorrhage were as follows; group A, $n = 7$; group B, $n = 3$; and group C, $n = 3$. Among the 3 patients assigned to group B, optic radiation was compressed by the hemorrhagic nidus in patient 22, was penetrating the hemorrhagic nidus in patient 25, and was not shifted or disrupted in another patient. Among the 3 patients assigned to group C, optic radiation was compressed by the hemorrhagic nidus in patients 29 and 34 and was not shifted or disrupted in another patient. Tractographic appearances are summarized in Table 2.

In patients without hemorrhage, AI of optic radiation volume ($P < .0001$), AI of perinidal FA along corticospinal tract ($P = .006$), and optic radiation ($P = .01$) differed significantly between groups. AI of corticospinal tract volume did not differ significantly between groups. In patients with hemorrhage, AI of perinidal FA ($P = .04$), tract volume ($P = .01$) of corticospinal tract, and AI of perinidal FA along optic radiation ($P = .004$) differed significantly between groups. AI of optic radia-

tion volume did not differ significantly between groups. Statistical results are summarized in Fig 3.

Discussion

The present study visualized the corticospinal tract and optic radiation tractography in patients with AVM and assessed the influence of intracranial AVM on tractography. DT imaging and fiber tractography techniques enable in vivo visualization of eloquent fiber tracts, a feat that is virtually impossible to achieve using conventional MR imaging techniques. Both 2D presentation of voxels where the fiber tract penetrates the section and 3D presentation of all of the tractographic images are useful for visualizing course changes of the fiber tract (Fig 2A,-B). Clinical application of tractography depends on the visualization of tractography in patients with intracranial space occupying the lesion. Our results show that, in patients without hemorrhage, perinidal FAs of both corticospinal tract and optic radiation were significantly different between the groups, and tract volume was significantly different only for the optic radiation between the groups. No patient experienced motor weakness, and no patient presented corticospinal tract disruption. One patient experienced right homonymous hemianopsia with disrupted optic radiation, though another

patient experienced lower left quadranopsia without disruption. The 2 other patients with disrupted optic radiation did not complain of any visual field defects.

In patients with brain tumor, corticospinal tract tractography has reportedly been disrupted as a result of tumor compression, direct involvement, or peritumoral edema.[4,17] In our results, perinidal FA along the 2 fiber tracts and optic radiation volume were significantly different between the 3 groups, though corticospinal tract volume did not significantly differ between the groups. In patients without neurologic deficit, corticospinal tract abutting the nidus was not disrupted in any patient, but optic radiation disruption abutting the nidus did not necessarily reflect visual field defect. Although nonhemorrhagic AVM has much less vasogenic edema, which seems to decrease diffusion anisotropy and subsequent FA values, our results show decreased perinidal FA in patients with nonhemorrhagic AVM. FA values of the eloquent fiber tracts near the nidus may reflect a change of microvasculature in normal-appearing white matter near the nidus. The different results from brain tumor and AVM are probably due to the pathologic nature of these 2 lesions. Even if the nidus could be deeply localized, particularly in the watershed lesions, AVM feeders are frequently superficial, and for the most part the actual vascular lesions are not infiltrating the white matter tract. The reasons for different results from the corticospinal tract and optic radiation tractography were probably related to technical difficulties in optic radiation tractography, as explained later in detail. Differences in anatomic features in the 2 fiber trajectories might also play a role. The corticospinal tract follows an anatomically coherent, colinear course between the centrum semiovale and cerebral peduncle. Conversely, the optic radiation is defined as a geniculocalcarine tract that begins at the lateral geniculate body, follows the lateral wall of the lateral ventricle into the temporal lobe, and terminates at the striate area on the medial surface of the occipital lobe on either side of the calcarine sulcus. However, course in the temporal lobe is intermingled with other fibers that course in various directions and are indistinguishable from surrounding fibers.[14] The optic radiations are not as coherent as corticospinal tract tractography, and these anatomic differences might have affected the results.

Hemorrhage associated with AVM induces vasogenic edema and susceptibility effects, and technical difficulties are considered likely to occur when performing tractography because of signal intensity drop-off in DT imaging, which is more prominent at 3T than at 1.5T. In the present cases with hemorrhagic AVM ($n = 13$), perinidal FA along the 2 fiber tracts and corticospinal tract volume were significantly different among the 3 groups, though optic radiation volume did not significantly differ among the groups. Four patients experienced motor weakness, including one patient whose corticospinal tract was veering laterally; fibers projecting from the medial precentral gyrus were disrupted; and the corticospinal tracts of the remaining 3 patients were not disrupted. No patient displayed disrupted optic radiation, though 3 patients suffered visual field defect or spatial neglect. These results are partly compatible with previous reports of white matter FA change in patients with brain tumor[4,17] or cerebral hemorrhage.[18,19] In our subjects, 8 patients had perifocal hyperintensity among the 13 hemorrhagic patients, which showed higher prevalence than nonhemorrhagic patients. Perifocal hyperintensity, including edema or gliosis, may have caused the FA change in the hemorrhagic subjects. Visually demonstrated "tract disruption" abutting the nidus did not necessarily reflect neurologic symptoms.

The present study reveals that perinidal FA and tract volume along the tract close to an AVM nidus are significantly lower than in the contralateral hemisphere. In contrast, tractographic appearance of "disruption" does not correlate with clinical symptoms, especially in patients associated with hemorrhage. Both the asymptomatic patient with disrupted tract (false-positive) and the symptomatic patient without tract disruption (false-negative) were present. This is probably due to the technical limitation of DT imaging and tractography induced by artifacts, including susceptibility effects. A decrease in perinidal FA along the tract or in tract volume reflects white matter change and subsequent clinical symptom more reliably than changes in tractographic appearances. Although clinical applications of tractography, such as functional evaluation or presurgical planning, should be performed carefully, relationships between eloquent fibers and AVMs have been visualized in patients with both hemorrhagic and nonhemorrhagic lesions. Attempts to validate the location of corticospinal tract tractography[20,21] and optic radiation tractography compared with electrophysiologic testing for motor or visual function are still under way.

Three major therapeutic strategies have been applied for intracranial AVM treatment: surgical operation, stereotactic radiosurgery, and endovascular embolization. Surgical treatment for intracranial AVM is challenging, given the need to manage obliteration of the nidus in addition to risk of intraoperative hemorrhage and postoperative edema or hemorrhage because of normal perfusion pressure breakthrough.[22] AVM operations are special in that palliative resection increases the risk of bleeding inversely in relation to the operation, and complete resection has always been required for surgical management of intracranial AVM,[23] whereas other intracranial space-occupying lesions receive partial resection to avoid postoperative neurologic deficits. Surgical indications for AVMs should thus be determined by considering the risk of postoperative deficits after complete resection. Locations of motor and visual pathways are more important for determining surgical indications of AVM near eloquent brain areas than other intracranial space occupying lesions, because an "all-or-nothing" operation is required for this condition. According to our results, both corticospinal tract and optic radiation tractography are supposed to be clinically feasible in considering the spatial distribution of eloquent fibers, though the correlation between tractographic appearance and clinical condition should be carefully interpreted. If surgical obliteration of an AVM is considered high risk because of the relationship between the lesion and eloquent white matter and eloquent cortices, alternative therapeutic strategies might be applied, such as stereotactic radiosurgery, endovascular embolization, or a combination of embolization and surgery.[24,25] DT tractography has been reported to be useful in confirming the radiation dose to the corticospinal tract during radiosurgical planning[26] and thus provides information for both therapeutic strategies and detailed planning.

The present study includes some limitations. First, techni-

cal difficulties in tractography may have affected the results. We applied a multiple ROI approach by using "OR," "AND," and "NOT" operations of choice. Although this approach is useful for known 3D configuration of white matter tract, and good agreement with postmortem anatomic studies has been reported,[2,27] "NOT" operations may lead to spurious elimination of tracts. At present, no tractography technique based on DT datasets visualizes fiber tracts of interest without any subjective ROI operations. Methods with greater precision and reproducible outcomes will be required in the future. Some differences in corticospinal tract tractography and optic radiation tractography also should be noted. Unlike cases with corticospinal tract, optic radiation tractography is more challenging. A number of authors have attempted to visualize the optic radiation tractography in different ways,[7,13,28,29] and no "gold standard" method has been established. No quantitative analysis methods for optic radiation tractography have yet been described. Measured parameters and analysis methods were based on the studies for corticospinal tract tractography, and the feasibility of parameters may remain questionable in optic radiation tractography. The second limitation is that tractography reconstruction is not a precise stepwise procedure with perfectly reproducible outcomes but is somewhat dependent on ROI manipulation and tracking algorithms. The FACT algorithm applied in this study is susceptible to a phenomenon known as "crossing fiber problems." New fiber-tracking algorithms have been applied to resolve such problems, and future technical advances will bring these new algorithms into clinical use. Optic radiation tractography by using probabilistic tractography techniques has been reported,[28] and this method might improve the difficulties associated with optic radiation tractography in the present study.

Conclusions

In patients with either hemorrhagic or nonhemorrhagic AVM, corticospinal tract and optic radiation tractography close to the nidus were less visualized in the affected hemisphere than those distant from the nidus. Tracts were less visualized in patients with neurologic symptoms than in asymptomatic patients. Fiber tractography for intracranial AVM visualizes relationships between eloquent fibers and AVM, and the information provided from eloquent white matter by fiber tractography may be useful for therapeutic strategies.

References

1. Basser PJ, Pajevic S, Pierpaoli C, et al. **In vivo fiber tractography using DT-MRI data.** *Magn Reson Med* 2000;44:625–32
2. Mori S, Crain BJ, Chacko VP, et al. **Three-dimensional tracking of axonal projections in the brain by magnetic resonance imaging.** *Ann Neurol* 1999;45:265–69
3. Pierpaoli C, Jezzard P, Basser PJ, et al. **Diffusion tensor MR imaging of the human brain.** *Radiology* 1996;201:637–48
4. Yamada K, Kizu O, Mori S, et al. **Brain fiber tracking with clinically feasible diffusion-tensor MR imaging: initial experience.** *Radiology* 2003;227:295–301
5. Clark CA, Barrick TR, Murphy MM, et al. **White matter fiber tracking in patients with space-occupying lesions of the brain: a new technique for neurosurgical planning?** *Neuroimage* 2003;20:1601–08
6. Yamada K, Kizu O, Ito H, et al. **Tractography for arteriovenous malformations near the sensorimotor cortices.** *AJNR Am J Neuroradiol* 2005;26:598–602
7. Kikuta K, Takagi Y, Nozaki K, et al. **Early experience with 3-T magnetic resonance tractography in the surgery of cerebral arteriovenous malformations in and around the visual pathway.** *Neurosurgery* 2006;58:331–37
8. Abe O, Yamada H, Masutani Y, et al. **Amyotrophic lateral sclerosis: diffusion tensor tractography and voxel-based analysis.** *NMR Biomed* 2004;17:411–16
9. Jiang H, van Zijl PC, Kim J, et al. **DtiStudio: resource program for diffusion tensor computation and fiber bundle tracking.** *Comput Methods Programs Biomed* 2006;81:106–16
10. Okada T, Miki Y, Fushimi Y, et al. **Diffusion-tensor fiber tractography: intra-individual comparison of 3.0-T and 1.5-T MR imaging.** *Radiology* 2006;238:668–78
11. Huang H, Zhang J, van Zijl PC, et al. **Analysis of noise effects on DTI-based tractography using the brute-force and multi-ROI approach.** *Magn Reson Med* 2004;52:559–65
12. Concha L, Gross DW, Beaulieu C. **Diffusion tensor tractography of the limbic system.** *AJNR Am J Neuroradiol* 2005;26:2267–74
13. Yamamoto A, Miki Y, Urayama S, et al. **Diffusion tensor fiber tractography of the optic radiation: analysis with 6-, 12-, 40- and 81-directional motion probing gradients; a preliminary study.** *AJNR Am J Neuroradiol* 2007;28:92–96
14. Kier EL, Staib LH, Davis LM, et al. **MR imaging of the temporal stem: anatomic dissection tractography of the uncinate fasciculus, inferior occipitofrontal fasciculus, and Meyer's loop of the optic radiation.** *AJNR Am J Neuroradiol* 2004;25:677–91
15. Thomalla G, Glauche V, Koch MA, et al. **Diffusion tensor imaging detects early wallerian degeneration of the pyramidal tract after ischemic stroke.** *Neuroimage* 2004;22:1767–74
16. Glenn OA, Henry RG, Berman JI, et al. **DTI-based three-dimensional tractography detects differences in the pyramidal tracts of infants and children with congenital hemiparesis.** *J Magn Reson Imaging* 2003;18:641–48
17. Lu S, Ahn D, Johnson G, et al. **Diffusion-tensor MR imaging of intracranial neoplasia and associated peritumoral edema: introduction of the tumor infiltration index.** *Radiology* 2004;232:221–28
18. Jang SH, Kwon YH, Lee MY, et al. **Corticospinal tract compression by hematoma in a patient with intracerebral hemorrhage: a diffusion tensor tractography and functional MRI study.** *Yonsei Med J* 2006;47:135–39
19. Salat DH, Smith EE, Tuch DS, et al. **White matter alterations in cerebral amyloid angiopathy measured by diffusion tensor imaging.** *Stroke* 2006;37:1759–64
20. Berman JI, Berger MS, Mukherjee P, et al. **Diffusion-tensor imaging-guided tracking of fibers of the pyramidal tract combined with intraoperative cortical stimulation mapping in patients with gliomas.** *J Neurosurg* 2004;101:66–72
21. Okada T, Mikuni N, Miki Y, et al. **Corticospinal tract localization: integration of diffusion-tensor tractography at 3-T MR imaging with intraoperative white matter stimulation mapping–preliminary results.** *Radiology* 2006;240:849–57
22. Spetzler RF, Martin NA, Carter LP, et al. **Surgical management of large AVM's by staged embolization and operative excision.** *J Neurosurg* 1987;67:17–28
23. Miyamoto S, Hashimoto N, Nagata I, et al. **Posttreatment sequelae of palliatively treated cerebral arteriovenous malformations.** *Neurosurgery* 2000;46:589–94
24. Söderman M, Andersson T, Karlsson B, et al. **Management of patients with brain arteriovenous malformations.** *Eur J Radiol* 2003;46:195–205
25. Pollock BE, Flickinger JC. **A proposed radiosurgery-based grading system for arteriovenous malformations.** *J Neurosurg* 2002;96:79–85
26. Maruyama K, Kamada K, Shin M, et al. **Integration of three-dimensional corticospinal tractography into treatment planning for gamma knife surgery.** *J Neurosurg* 2005;102:673–77
27. Wakana S, Jiang H, Nagae-Poetscher LM, et al. **Fiber tract-based atlas of human white matter anatomy.** *Radiology* 2004;230:77–87
28. Powell HW, Parker GJ, Alexander DC, et al. **MR tractography predicts visual field defects following temporal lobe resection.** *Neurology* 2005;65:596–99
29. Taoka T, Sakamoto M, Iwasaki S, et al. **Diffusion tensor imaging in cases with visual field defect after anterior temporal lobectomy.** *AJNR Am J Neuroradiol* 2005;26:797–803